

Affordance-Guided Reinforcement Learning via Visual Prompting

Olivia Y. Lee¹, Annie Xie¹, Kuan Fang², Karl Pertsch^{1,2}, Chelsea Finn¹

¹Stanford University, ²UC Berkeley

oliviyal@stanford.edu

Abstract—Robots equipped with reinforcement learning (RL) have the potential to learn a wide range of skills solely from a reward signal. However, obtaining a robust and dense reward signal for general manipulation tasks remains a challenge. Existing learning-based approaches require significant data, such as demonstrations or examples of success and failure, to learn task-specific reward functions. Recently, there is also a growing adoption of large multi-modal foundation models for robotics. These models can perform visual reasoning in physical contexts and generate coarse robot motions for various manipulation tasks. Motivated by this range of capability, in this work, we propose and study rewards shaped by vision-language models (VLMs). State-of-the-art VLMs have demonstrated an impressive ability to reason about affordances through keypoints in zero-shot, and we leverage this to define dense rewards for robotic learning. On a real-world manipulation task specified by natural language description, we find that these rewards improve the sample efficiency of autonomous RL and enable successful completion of the task in 20K online finetuning steps. Additionally, we demonstrate the robustness of the approach to reductions in the number of in-domain demonstrations used for pretraining, reaching comparable performance in 35K online finetuning steps.

I. INTRODUCTION

Recent advances in large language models (LLMs) and vision-language models (VLMs) trained on Internet-scale data show promising results in using commonsense understanding to plan and reason [37, 8, 1, 38, 25]. They can break down complex instructions provided in natural language into actionable task plans [9, 5, 2, 6, 18, 19], perform visual reasoning in a variety of contexts [50, 7, 36], and even generate coarse robot motions for simple manipulation tasks [5, 34, 46, 18, 20, 36]. However, current state-of-the-art models still struggle with understanding interactions and physical dynamics in 3D space, which is essential to robotic control. Determining how to ground such models in the specific embodiment and environment dynamics remains a significant challenge. Several prior works have utilized large pretrained models for robotic control, either through few-shot prompting or finetuning of large models to generate actions directly [5], plans [1, 19, 18], or code [26, 27]. However, finetuning these models typically requires extensive human supervision, such as teleoperated demonstrations, feedback on whether the task was successfully completed, or a predefined set of skills and their controllers.

An alternative paradigm for finetuning robotic policies is autonomous reinforcement learning (RL), which only requires a reward signal to refine the robot’s behavior and can therefore require less supervision in comparison. A significant amount

of recent work has also focused on improving the sample-efficiency of these algorithms by pretraining on large offline datasets [23, 3, 22, 24, 32, 51]. Despite these advances, obtaining a reward signal is still a non-trivial problem, that requires either careful engineering or large amounts of data to learn a robust reward function [17, 13, 14, 47, 41]. The application of pretrained VLMs for defining rewards is therefore attractive, but thus far, they have primarily been used for generating sparse rewards [31, 44, 51], which often leads to less efficient learning. VLMs hold much richer and denser knowledge that we can elicit, such as reasoning about the affordances of various objects and environments. In this work, we leverage this understanding to shape rewards for robotic RL.

Specifically, we present a method for open-vocabulary visual prompting to extract rewards from VLMs for online RL. We leverage insights on effective visual prompting methods from Liu et al. [28] to develop a method for generating keypoints and waypoint trajectories from which dense shaping rewards can be calculated. We integrate the pipeline of extracting affordance representations from VLMs and computing dense rewards into RoboFuME [51], an autonomous RL system that uses sparse rewards from a finetuned VLM. We demonstrate comparable success rates on a variety of complex object manipulation tasks used in RoboFuME, as well as improved success rates on new tasks that the existing pipeline struggles to generalize to using sparse rewards alone, with reduced reliance on in-domain expert demonstrations.

II. RELATED WORK

A. Foundation Models for Robotics

The rapid development of foundation models in recent years has drawn significant attention both in the academic community and beyond [12]. This surge of interest in foundation models has arisen because they demonstrate that models trained on broad, Internet-scale data are highly adaptable to a wide range of downstream tasks. Robotics is a specific downstream task of foundation models that has garnered a lot of interest in the academic community. Works like SayCan [1] demonstrate encouraging results in training language-conditioned robotic control policies. Such approaches allow us to leverage and ground the rich knowledge and reasoning capabilities of LLMs to enable embodied agents to complete long-horizon tasks.

While the results from SayCan [1] seem promising, there is a critical engineering risk that the reasoning abilities and

representations captured by LLMs are overly general for embodied tasks, and more work is needed to properly ground the high-level plans generated by LLMs in low-level actions for embodied tasks. Converting visual observations into language descriptions and planning in solely in the language space loses a lot of rich information critical to scene understanding, which is a major limitation of using LLMs for spatial planning, reasoning, and task completion. Notably, the ELLM system from Du et al. [10] generated inaccurate responses to whether objects matched the goal positions when tasked with rearranging objects in a household environment to match the goal arrangement. It is important to pay attention to the pitfalls in the household environment despite the successes in the open-world Crafter environment. The goals for survival in an open-world environment (such as `build house`, or `acquire food`) are fairly general and transferable, and LLMs have likely encountered such scenarios during training and can suggest reasonable goals. However, the general knowledge encoded in LLMs may not necessarily be as beneficial for robot learning: LLMs can provide general priors for planning and reasoning, but this generality also results in reduced specificity to the environment that the robot is operating in, thus the general priors may require additional grounding.

Therefore, planning solely with language thus loses a lot of information associated with the richness of the visual modality that is critical to most robotics applications. Our work explores leveraging the visual modality via state-of-the-art VLMs to facilitate reasoning in both language and image domains.

B. Vision-Language Models

The clear advantage of language is the natural interface for providing task instructions and describing goals. That said, much of robotics research relies heavily on accurately perceiving and interacting with the environment. Several state-of-the-art VLMs [33, 49, 29, 39] demonstrate highly generalizable open-vocabulary object localization. However, they still lack the extensive reasoning capabilities of LLMs, since reasoning over image inputs is significantly more complicated. Preliminary VLMs require text queries where the objects involved are known *a priori* to generate bounding boxes around the requested objects, which are then provided to LLMs for downstream reasoning. Modern VLMs, such as GPT-4V [52] and Gemini [15], have demonstrated promising capabilities in combining LLM reasoning with environment perception via visual inputs. A key advantage of using modern VLMs is that it simplifies the process of translating high-level plans into low-level robot actions. While previous works leveraging LLMs like SayCan [1] require pretrained skill policies for each action primitive, using modern VLMs can circumvent the issue of selecting from a suite of pretrained action policies, by deriving rewards from image space that can be used for learning state-action mappings via RL. This is because VLMs, unlike LLMs, can determine success or failure based on image observations, and this reward signal can be used to enable robots to learn through trial-and-error, without training skill policies via imitation learning which are costly and difficult to

scale. VLMs can also guide the learning process by generating shaping rewards, in the form of intermediate waypoints.

Defining rewards in image space by using VLMs to determine task completion and specify intermediate waypoints as goals is a key contribution of our work. A major engineering challenge is tuning the inputs to these VLMs, which are highly expressive but also opaque, to derive useful reward signals for learning. Both language and image prompts require careful tuning to generate accurate and meaningful outputs, as we have found that modern VLMs still struggle to some degree with spatial reasoning. Our work explores combining preliminary VLMs and modern VLMs, as the outputs (bounding boxes or segmentations) of preliminary VLMs can serve as more helpful inputs to modern VLMs for semantic reasoning than raw image observations, thereby leveraging pretrained representations in VLMs as reward predictors.

C. Autonomous Reinforcement Learning

Online RL is the paradigm by which agents gather data through interaction with the environment, then store this experience in a replay buffer and update its policy based on this experience. This contrasts with offline RL, where the agent updates its policy using previously collected data or human demonstrations, without itself interacting with the environment. A longstanding goal is autonomous RL: the potential of placing a robot in a real-world environment and it improves on its own by autonomously gathering in-domain experience, which holds great promise for scalable robot learning. In autonomous RL, the agent not only learns through its own experience, but also does not require human supervision to reset the environment between trials [40].

Algorithms for autonomous RL have been difficult to implement in the real world, with the primary challenge being sample complexity, the number of calls to the model required to achieve acceptably good performance. In addition, there is the challenge of providing well-shaped rewards for online exploration, as well as the difficulty of continual reset-free training, which requires significant human effort. Several works have developed systems for reset-free training to reduce or eliminate human interventions in the online RL process [4, 51, 16, 42], but reward engineering is an open problem as manually specified reward signals are seen as difficult to engineer and easy to exploit, and autonomous RL suffers when the reward signal is too sparse. While hand-designing reward functions is challenging, there is great potential to learn reward functions from previously collected data or extract rewards from large pretrained models. Some works have attempted to learn rewards from human feedback [43, 4], while acknowledging that these rewards are noisy and still require human intervention. The large bank of offline image and video datasets, as well as the high inference speed and accessibility of large pretrained models, could potentially offer solutions to further reduce or eliminate human intervention, while providing more precise and informative shaping rewards.

There has been attempts to leverage VLMs to generate rewards for online RL. RoboFuME [51] finetunes MiniGPT-

4 [54] to generate task completion rewards on a moderate number of in-domain demonstrations. However, these rewards are still sparse and pretraining requires a substantial number of in-domain demonstrations per task, which is costly and also makes the system more brittle and less robust to generalization. We also draw upon recent work extracting rewards from LLMs [30, 53] and VLMs to guide zero-shot robotic manipulation [28, 44, 31] and online adaptation [51, 48]. In particular, our work investigates leveraging affordance-based representations from VLMs to tackle the dense reward shaping problem.

III. METHODOLOGY

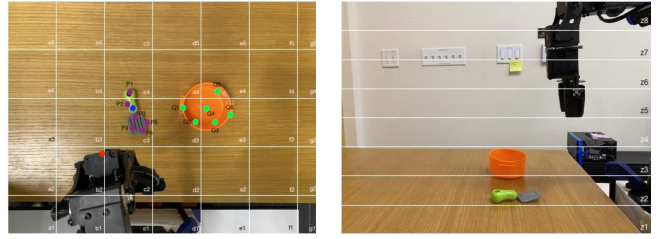
A. Problem Statement

We consider problems that can be formulated as a partially observable Markov Decision Process (POMDP) tuple $(\mathcal{S}, \mathcal{A}, \mathcal{O}, \gamma, f, p, r, d_0)$ where \mathcal{S} is the state space, \mathcal{A} is the action space, \mathcal{O} is the observation space, $\gamma \in (0, 1)$ is the discount factor, $r(s, a)$ is the reward function and $d_0(s)$ is the initial state distribution $d_0(s)$. The dynamics are governed by a transition function $p(s'|s, a)$. The observations are generated by an observation function $f(o|s)$. The goal of RL is to maximize the expected sum of discounted rewards $\mathbb{E}_\pi[\sum_{t=1}^{\infty} \gamma^t r(s_t, a_t)]$. In this work, we use RGB image-based observations. The reward function is typically hand-engineered or learned, for instance via examples of task success and failure [17, 13, 14, 47, 41, 51]. We assume the existence of a sparse task completion reward (that is, $r(s, a) \in \{0, 1\}$), which can be acquired with systems like RoboFuME [51].

B. Reward Shaping via VLM-Generated Keypoints

A sparse reward is typically easier to specify but, with it, RL algorithms typically require more samples to learn a successful policy, because it requires the agent to encounter success through its own exploration. In comparison, a dense reward provides a continuous form of feedback that guides the agent towards success. Our method aims to provide the latter type of feedback by augmenting sparse task completion rewards with a dense shaping reward term. Specifically, this dense reward is calculated with respect to a sequence of intermediate waypoints marking trajectory points towards the goal. This can be seen as breaking down a trajectory into short sub-trajectories or subtasks that are more easily reachable by the agent. Such guidance can facilitate learning of more complex and longer-horizon manipulation tasks compared to the sparse reward signal alone.

At a high-level, to define dense rewards, we require waypoints that form a coarse trajectory of how the robot should complete the task. We leverage GPT-4V to generate these predictions through recently proposed visual prompting techniques [28]. In addition to waypoints, we also prompt GPT-4V to select appropriate grasp and target points for the manipulation task, which we find especially important for success in our experiments. After these points are generated, we assign rewards to each timestep of an RL episode based on how well it follows this trajectory. We provide specific implementation details of this method below:



(a) Top-down view, annotated with grid labels and keypoints. (b) Side view, annotated with line labels.

Fig. 1: Example annotated inputs to GPT-4V.

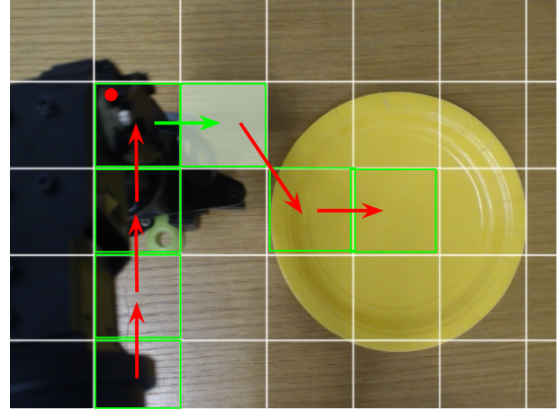


Fig. 2: Example of a GPT-4V generated trajectory: tiles marked by green borders and red arrows indicate direction of movement. The current robot position computed by RANSAC prediction is labeled by the red point. Our dense reward formulation encourages the robot to move to the next block, following the direction of the green arrow.

- 1) *Generating sequence of waypoints and grasp point:* We take the first observation in the episode o_0 , which consists of a top-down image o_0^d and the side view image o_0^s . Our goal is to create a candidate set of grasp points and keypoints that GPT-4V can select from. Therefore, we preprocess these images by (1) passing o_0^d through GroundingSAM to get segmentations of relevant objects and sample six points from their masks, and (2) overlaying a grid and the sampled grasp points on top of o_0^d to get \tilde{o}^d . For the side-view image, we augment o_0^s with a series of evenly-spaced labeled horizontal lines to get \tilde{o}^s , to provide depth information that is excluded from the top-down view. See Figure 1 for an example.

We pass \tilde{o}^d and \tilde{o}^s , together with a language instruction and metaprompt (Appendix E3) to GPT-4V, which generates several outputs but most important among them is `block_sequence`. This sequence is a list of tuples (x, y, z) , where (x, y) is a grid point chosen from \tilde{o}^d representing a position in the xy-plane from top-down and z is a line chosen from \tilde{o}^s representing a position in the z-axis from the side view. The dense rewards are calculated with respect to `block_sequence` in the next step.

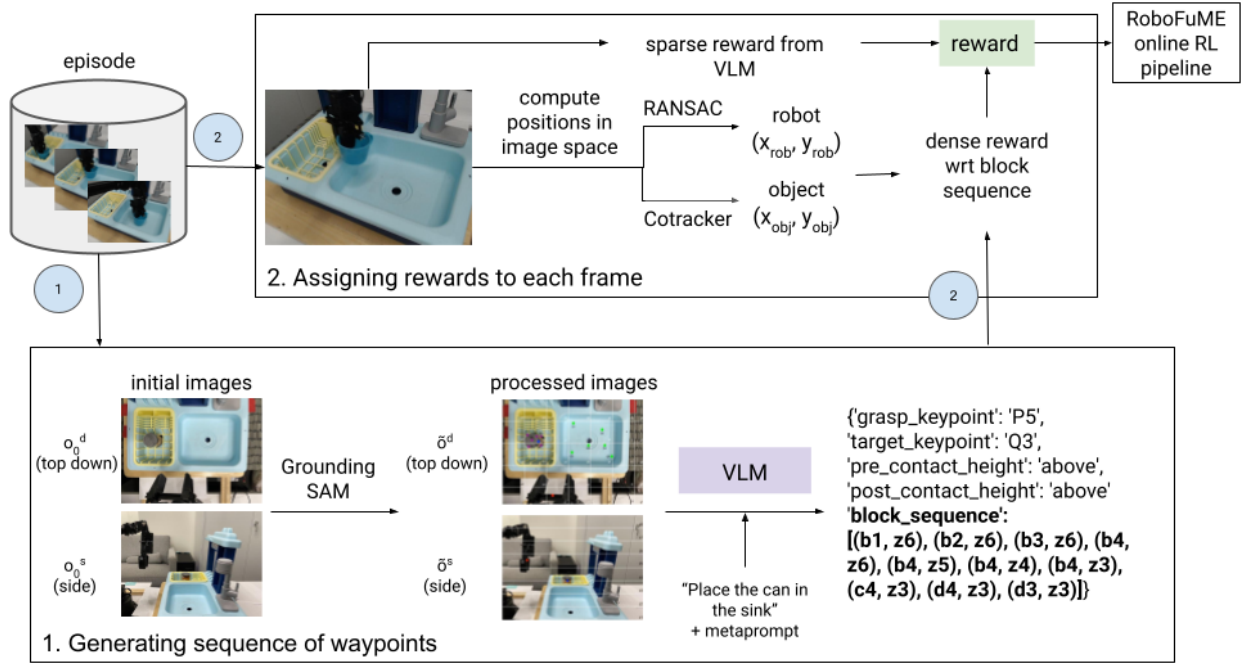


Fig. 3: Our method consists of two components. The first (represented by arrow (1) above) leverages GPT-4V to generate a sequence of waypoints. The second (represented by arrows (2) above) involves per timestep reward computation for each frame in the replay buffer, computing reward with respect to the waypoint sequence and a sparse reward derived from zero-shot VLM inference. The dense reward is used for online RL if the sparse reward is 0, else the sparse reward is used.

2) *Assigning rewards to each frame of an episode:* For each frame in the episode, we compute the positions of the robot and object in image space. We use a fitted RANSAC regressor to compute the robot position (x_{rob}^t, y_{rob}^t) . Optionally, we can also use an off-the-shelf pixel tracker [21] to track a specific point on the object (x_{obj}^t, y_{obj}^t) if we want to additionally define the rewards based on object poses. Using these coordinates, we compute the nearest block to each of the robot and object position in `block_sequence`, B_{rob}^i and B_{obj}^i respectively (see Figure 2 for an example). We can now compute a reward based on the robot and object positions, where r_{rob}^t is based on the negative L2 distance from the robot to the *block after the closest block in `block_sequence`*, B_{rob}^{i+1} , and correspondingly for the object, B_{obj}^{i+1} . We use the next block to encourage progression towards the goal, instead of stagnating at the current position. We further transform the distance by applying a tanh function so that the reward is between 0 and 1: $r_t = 0.5 \cdot (1 - \tanh(\text{dist}))$. To summarize, the reward is 1 when the sparse reward is 1, otherwise it is our dense reward. This reward is then optimized with an online RL algorithm.

C. Overall Autonomous RL Pipeline

To optimize this reward, we build on top of the RoboFuME system [51], an autonomous RL pipeline that can learn from image observations without environment resets. The proposed system requires a dataset of in-domain demonstrations (50

demonstrations of the forward and backward task each). RoboFuME then pretrains a policy on this data and examples from the Bridge dataset [11, 45]. It also fine-tunes MiniGPT-4 [54] as a sparse reward function using these demonstrations and additional 20 examples of failures. In our experiments, we show that the system can learn from significantly fewer in-domain demonstrations thanks to our dense rewards.

To summarize, the motivation for using dense shaping rewards generated by GPT-4V is to (1) augment the sparse task completion reward with a signal rewarding the agent for reaching intermediate waypoints thereby guiding task completion, and (2) reduce the reliance on in-domain demonstrations in the pipeline by getting fairly generalizable rewards from a large pretrained VLM. This approach is also highly flexible, as the VLM used in the pipeline can easily be replaced with a more advanced iteration of GPT or even other model families like Gemini [15] with little or no modifications to the metaprompt, based on preliminary experiments.

IV. EXPERIMENTS

We design our experiments to answer the following question: do our dense rewards make online reinforcement learning more efficient? As initial steps, we reproduce the results from the original RoboFuME work [51] in Appendix A and verify that dense rewards are helpful in simulation in Appendix C. We further test whether dense reward shaping can reduce the system's dependence on in-domain demonstrations. These experiments demonstrate that by adding dense shaping rewards,

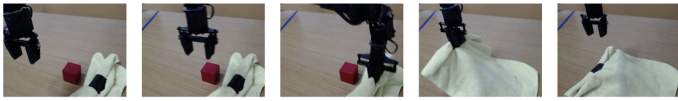


(a) Cloth Folding forward trajectory.



(b) Cloth Folding backward trajectory.

Fig. 4: Cloth Folding trajectories.



(a) Cube Covering forward trajectory.



(b) Cube Covering backward trajectory.

Fig. 5: Cube Covering trajectories.



(a) Spatula Pick-Place forward trajectory.



(b) Spatula Pick-Place backward trajectory.

Fig. 6: Spatula Pick-Place trajectories.

online RL pipelines like RoboFuME can better learn new tasks, especially since the dense rewards are obtained using VLMs with significant generalization capabilities.

A. Experimental Setup

We used the following tasks for our experiments: Cloth Folding, Cube Covering, and Spatula Pick-Place. The former two tasks were introduced in RoboFuME, and we use them here to demonstrate successful reproduction of RoboFuME as a benchmark and for ablation tests to demonstrate the necessity of in-domain demonstrations for the pipeline (Appendix A). For Spatula Pick-Place, we demonstrate the challenges of reproducing RoboFuME on novel tasks and the use of dense shaping rewards to overcome this generalization problem and reduce reliance on in-domain demonstrations.

In RoboFuME, only subsets of the Bridge dataset were used to pretrain policies with language-conditioned BC and offline RL. For the two tasks also used in RoboFuME, we used the same Bridge data subsets, mostly featuring cloth-related tasks. For the novel Spatula Pick-Place task, we explore the selection

of these subsets of Bridge data in Appendix B. To ensure effective transfer learning from Bridge data, the camera angle and setup for the in-domain demonstrations were made highly similar to the camera angles used in the Bridge data.

Visualizations of the in-domain demonstrations collected for the forward and backward task of each task category are included for Cloth Folding (Figure 4), Cube Covering (Figure 5), and Spatula Pick-Place (Figure 6). Policies were pretrained using language-conditioned BC and offline RL on the standard quantity of in-domain demonstrations (50 forward task trajectories, 50 backward task trajectories, and 20 mixed-mode failures). As done in RoboFuME, the forward and backward trajectories were collected with minimal multimodality and randomization, to facilitate reset-free RL. After pretraining on Bridge and in-domain data using offline RL, policies are finetuned online using CaQL [35] for 20K steps. While RoboFuME claimed to enable minimal resets (every 10-15 episodes), since reset-free learning was not an emphasis of our method, we reset the model every 2 episodes to maximize useful interactions and speed up the learning process.

For the experiments in Section IV-B, the model was pretrained on the standard quantity of in-domain demonstrations. The pretrained models (with language-conditioned BC and offline RL) as well as the offline RL models finetuned online for 20K steps were evaluated on success out of 20 trials each of the forward and backward tasks in each task category. For the experiments in Section IV-C, the model was pretrained on a set of in-domain demonstrations reduced by 5x from the standard quantity, and finetuned for 20K steps and further until 35K steps to understand the system’s robustness to reduced in-domain demonstrations.

Success was evaluated qualitatively by similarity to the in-domain demonstrations collected: for Cloth Folding, the cloth had to be folded or unfolded to a degree similar to the expert demonstrations; for Cube Covering, the entire cube had to be covered or uncovered from the camera perspective shown in Figure 5; for Spatula Pick-Place, the spatula had to be on the yellow plate (forward task) or on the left side of the plate close to where it was picked originally (backward task).

The full approach for dense reward shaping is detailed in Section III-B. For implementation on the real robot, we use a modified version of the approach using 2D waypoint guidance from a top-down camera, and track only the robot gripper’s position by RANSAC prediction using robot proprioception. Because the environment is manually reset after every two episodes (one forward and one backward episode), we query GPT-4V once at the beginning of the experiment to generate the intermediate waypoints for the forward and backward tasks, and use those waypoints for all forward and backward episodes. We finetune MiniGPT-4 to generate sparse rewards, as done in RoboFuME [51], and finetune different versions depending on the number of in-domain demonstrations used during pretraining, to investigate the robustness of the method to different quantities of in-domain demonstrations.

From the GPT-4V generated waypoint trajectory, we use the centroid of each grid tile to create a trajectory of pixel

Method	Behavior Cloning	RL Pretraining Only	Sparse Rewards (RoboFuME)	Dense Rewards (Ours)
Without in-domain demos	0%	0%	5%	—
With in-domain demos	30%	25%	40%	45%

TABLE I: Results of finetuning policies online for 20K steps with sparse only vs. sparse and dense rewards for Spatula Pick-Place task. Policies labeled bridge + indomain were pretrained on the standard quantity of in-domain demonstrations in RoboFuME [51].

coordinates in image space. We use calculate the negative L2 distance between the current robot position and the target waypoint (initialized as the first waypoint in the VLM-generated sequence), changing the target waypoint to the next one in the sequence to encourage progress along the trajectory. We pass each distance through a modified tanh function, so $r_{\text{dense}} = 0.5(1 - \tanh(\lambda(d_t - \varphi)))$, where d_t is the negative L2 distance between the robot position and the target waypoint at timestep t , and scaling factor λ and offset φ are hyperparameters. We set $\lambda = -0.02$ and $\varphi = 120$ for the results reported in Table I. This ensures the dense reward stays between 0 and 1, with values closer to 1 when the robot trajectory is closer to the VLM-generated waypoint trajectory. What distinguishes trajectories that stay close to the VLM-generated trajectories and truly good trajectories that complete the task is the sparse reward. We set the final reward for each timestep $r = r_{\text{sparse}}$ if $r_{\text{sparse}} = 1$ else $r = r_{\text{dense}}$.

B. Finetuning with Dense Rewards

We pretrain policies for Spatula Pick-Place on a curated subset of the Bridge dataset (see Appendix B). The offline RL policy pretrained on Bridge and high-quality in-domain demonstration data achieves 25% success rate. For our RoboFuME comparison, we finetune this policy online for 20K steps using only VLM-generated sparse rewards, with resets every 2 episodes to maximize meaningful online interactions. For our method, we finetune this policy online for 20K steps using both VLM-generated sparse rewards and dense rewards calculated with respect to a VLM-generated waypoint trajectory, also with resets every 2 episodes.

The results are shown in Table I. After finetuning with just VLM-generated sparse rewards, the performance of the offline RL policy pretrained on Bridge and in-domain data increases from 25% to 40%. While this is lower than the success rate of cloth tasks in Appendix A, the increase in success rate with finetuning using sparse rewards is comparable to a Pot Pick-Place task from Yang et al. [51], and both Pick-Place tasks are considerably harder than the cloth tasks. After finetuning with VLM-generated sparse rewards and dense shaping rewards, the performance of the offline RL policy pretrained on Bridge and in-domain data further increases to 45%. This is comparable to the success rate of RoboFuME in the Pot Pick-Place task after finetuning with 30K steps using only sparse rewards.

While the increase in success rate finetuning with dense and sparse rewards vs. just sparse rewards is not extremely significant, the qualitative behavior observed was better, with representative image sequences demonstrating policy performance on the real robot shown in Figure 7. The policy finetuned with sparse rewards, while fairly successful, com-

monly demonstrated the behavior shown in Figure 7a where the spatula was dropped onto the plate from a high height, rather than lowering and placing the spatula as done in the demonstrations. The robot gripper also continues moving to the right rather than hovering above the placement point, indicating several coincidental successes. On the other hand, the policy finetuned with dense rewards, while only slightly more performant success rate-wise, demonstrated better qualitative behavior shown in Figure 7b, lowering the spatula onto the plate and hovering above the placement point, as done in the demonstrations. This is likely due to dense rewards shaping the behavior to be more like the GPT-4V generated trajectory.



(a) Qualitative behavior of policy finetuned only on sparse rewards: Robot drops spatula on the plate from a height and continues moving rightward.



(b) Qualitative behavior of policy finetuned only both dense and sparse rewards: Robot lowers and place spatula on the plate and subsequently hovers above the placement position.

Fig. 7: Qualitative behavior of policies finetuned on sparse only vs. dense and sparse rewards.

C. Robustness to Reducing In-Domain Demonstrations

In Table I, the policy trained via offline RL on Bridge data only, without any in-domain demonstrations, struggles to make meaningful progress towards task completion. This suggests that RoboFuME is highly reliant on in-domain demonstrations, however this introduces a notable cost of collecting in-domain demonstrations for each new task. We investigate the effect of reducing the number of in-domain demonstrations used during pretraining on the policy’s ability to successfully learn during online finetuning. We then evaluate whether our dense rewards can reduce the system’s reliance on in-domain demonstrations, thereby reducing its brittleness.

We pretrain a policy via offline RL on 5x less than the standard quantity of in-domain demonstrations (10 forward tasks, 10 backward tasks, and 2 failures). We finetune this policy online for 20K steps using sparse rewards only as well as sparse and dense rewards, then until 35K steps as the sparse reward only policy seemed to be plateauing while the sparse and dense reward policy still showed signs of improvement.

Pretrained RL policy	Sparse only, 20K steps	Dense, 20K steps (Ours)	Sparse only, 35K steps	Dense, 35K steps (Ours)
10%	15%	30%	15%	40%

TABLE II: Results of finetuning policies online for 20K and 35K steps with sparse only vs. sparse and dense rewards for Spatula Pick-Place task. Policies were pretrained on 5x less than the standard quantity of in-domain demonstrations in RoboFuME [51].

The results are shown in Table II. As expected, the pre-trained policy without any finetuning does very poorly on the task, and worse than the policy pretrained via RL on Bridge data and the standard quantity of in-domain demonstrations (column 4 of Table I). After finetuning for 20K steps, using only sparse rewards only marginally improves success rate. The robot often struggles to either grasp the spatula or place it on the plate. However, the dense reward formulation notably improves success rate to 30%, with the dense reward shaping its behavior. Qualitative analysis suggested there was still room for improvement, so we continued to finetune the policy for an additional 15K steps to see if we could recover the success rates of the policies trained on the standard quantity of demonstrations. The sparse reward only policy plateaued both in success rate (15%) and qualitative behavior, while the policy finetuned with dense rewards continued to learn and achieved a success rate of 40%, recovering the performance of RoboFuME finetuned policy on the full set of in-domain demonstrations (column 6 of Table I). This shows potential for using dense shaping rewards to reduce reliance on in-domain demonstrations during and facilitate better generalization of autonomous RL pipelines like RoboFuME to new tasks.

Another notable change in performance resulting from reducing in-domain demonstrations was finetuning MiniGPT-4. The sparse reward predictions of MiniGPT-4 were significantly worse using the reduced set of in-domain demonstrations, since there was less in-domain data to finetune the sparse reward predictor on. This contributed to challenges finetuning on sparse rewards only, since the predicted rewards were less accurate. To mitigate this and eliminate the confounding factor of inaccurate sparse rewards, we modified the sparse reward computation such that the reward predictor took four task-completion prompts as input (e.g., ‘Is the spatula on the plate?’, ‘Has the spatula been moved to the plate?’, etc.), and had to reach a consensus across all prompts to generate a sparse reward of 1. This approach generated sensible sparse rewards, though the sparse reward only approach still failed to successfully learn with reduced in-domain demonstrations, potentially attributable to pretraining the policy on fewer demonstrations. Nonetheless, this reveals another source of fragility in the system, as finetuning MiniGPT-4 is heavily reliant on in-domain demonstrations to generate accurate sparse rewards which are crucial for online RL. Leveraging larger models like GPT-4V zero-shot to extract sparse task completion rewards may help to circumvent this issue.

Overall, the quantitative results in Table I and qualitative results in Figure 7 collectively suggest that dense shaping re-

wards extracted from GPT-4V can help facilitate generalization of online RL pipelines like RoboFuME to new tasks where only using sparse rewards would not be able to generalize as well. Furthermore, the results in Table II suggest that policies finetuned with dense rewards are more robust to reducing the quantity of in-domain demonstrations, unlike policies finetuned only on sparse rewards.

V. CONCLUSION & FUTURE WORK

Our experiments present several insights into the opportunities and challenges of autonomous RL pipelines, and the potential for mark-based visual prompting to improve generalization capabilities of robotic agents equipped with RL. In particular, we explore the challenges of using only sparse rewards for online finetuning and relying on in-domain demonstrations with low multimodality to successfully pretrain policies of online RL. Approaches using only sparse rewards are slower to learn to complete tasks, and approaches reliant on in-domain demonstrations are much more brittle and less robust to generalizing to new tasks, objects, and environments.

We demonstrate that dense shaping rewards extracted from VLMs can help to speed up online RL, and facilitate generalization to new tasks where only relying on sparse rewards may not do as well. Leveraging both dense and sparse rewards facilitated improved learning, with better robustness to reduced in-domain demonstrations than just sparse rewards. Our reward formulation could be a possible modification to make existing finetuning methods more robust to changes in tasks, objects, and environments. We have demonstrated the benefits of dense shaping rewards extracted from VLMs, and open up new avenues of exploration to leverage the generalization capabilities of VLMs to enhance the robustness of robot learning systems.

There are several areas for future work. First, adding a side camera view for depth information will be crucial for more complex tasks. Dense rewards computed using 3D waypoints instead of 2D may better facilitate complex manipulation tasks but adds complexity to the system, so dense reward calculation must be tuned to account for this. Next, sparse task completion rewards can be seen as high-level tracking of object position (i.e., whether the object moved to the target location or not); implementing waypoint trajectories for object tracking and incorporating this into dense reward computation could further shape robot behavior and expedite learning. In addition, running large models like GPT-4V after every episode to generate dense waypoint trajectories and sparse rewards might be more accurate, but may also suffer from latency issues, and future work can explore this tradeoff to speed up the online finetuning process and facilitate scalability of the method to more complex tasks and environments. Further hyperparameter tuning in the dense reward computation algorithm (namely scaling factor λ and offset φ in the reward formulation above) as well as in the CalQL algorithm could further improve the success rate of policies finetuned with dense and sparse rewards. Overall, these future research directions can help efficiently scale autonomous RL systems to a greater diversity of complex tasks with different objects and environments.

REFERENCES

- [1] Michael Ahn, Anthony Brohan, Noah Brown, Yevgen Chebotar, Omar Cortes, Byron David, Chelsea Finn, Chuyuan Fu, Keerthana Gopalakrishnan, Karol Hausman, Alex Herzog, Daniel Ho, Jasmine Hsu, Julian Ibarz, Brian Ichter, Alex Irpan, Eric Jang, Rosario Jauregui Ruano, Kyle Jeffrey, Sally Jesmonth, Nikhil J Joshi, Ryan Julian, Dmitry Kalashnikov, Yuheng Kuang, Kuang-Huei Lee, Sergey Levine, Yao Lu, Linda Luu, Carolina Parada, Peter Pastor, Jornell Quiambao, Kanishka Rao, Jarek Rettinghouse, Diego Reyes, Pierre Sermanet, Nicolas Sievers, Clayton Tan, Alexander Toshev, Vincent Vanhoucke, Fei Xia, Ted Xiao, Peng Xu, Sichun Xu, Mengyuan Yan, and Andy Zeng. Do as i can and not as i say: Grounding language in robotic affordances. 2022.
- [2] Michael Ahn, Anthony Brohan, Noah Brown, Yevgen Chebotar, Omar Cortes, Byron David, Chelsea Finn, Chuyuan Fu, Keerthana Gopalakrishnan, Karol Hausman, et al. Do as i can, not as i say: Grounding language in robotic affordances. *arXiv preprint arXiv:2204.01691*, 2022.
- [3] Nair Ashvin, Dalal Murtaza, Gupta Abhishek, and L Sergey. Accelerating online reinforcement learning with offline datasets. *CoRR*, vol. *abs/2006.09359*, 2020.
- [4] Max Balsells, Marcel Torne, Zihan Wang, Samedh Desai, Pulkit Agrawal, and Abhishek Gupta. Autonomous robotic reinforcement learning with asynchronous human feedback, 2023.
- [5] Anthony Brohan, Noah Brown, Justice Carbajal, Yevgen Chebotar, Xi Chen, Krzysztof Choromanski, Tianli Ding, Danny Driess, Avinava Dubey, Chelsea Finn, et al. Rt-2: Vision-language-action models transfer web knowledge to robotic control. *arXiv preprint arXiv:2307.15818*, 2023.
- [6] Boyuan Chen, Fei Xia, Brian Ichter, Kanishka Rao, Keerthana Gopalakrishnan, Michael S Ryoo, Austin Stone, and Daniel Kappler. Open-vocabulary queryable scene representations for real world planning. In *2023 IEEE International Conference on Robotics and Automation (ICRA)*, pages 11509–11522. IEEE, 2023.
- [7] Boyuan Chen, Zhuo Xu, Sean Kirmani, Brian Ichter, Danny Driess, Pete Florence, Dorsa Sadigh, Leonidas Guibas, and Fei Xia. Spatialvlm: Endowing vision-language models with spatial reasoning capabilities. *arXiv preprint arXiv:2401.12168*, 2024.
- [8] Aakanksha Chowdhery, Sharan Narang, Jacob Devlin, Maarten Bosma, Gaurav Mishra, Adam Roberts, Paul Barham, Hyung Won Chung, Charles Sutton, Sebastian Gehrmann, Parker Schuh, Kensen Shi, Sasha Tsvyashchenko, Joshua Maynez, Abhishek Rao, Parker Barnes, Yi Tay, Noam Shazeer, Vinodkumar Prabhakaran, Emily Reif, Nan Du, Ben Hutchinson, Reiner Pope, James Bradbury, Jacob Austin, Michael Isard, Guy Gur-Ari, Pengcheng Yin, Toju Duke, Anselm Levskaya, Sanjay Ghemawat, Sunipa Dev, Henryk Michalewski, Xavier Garcia, Vedant Misra, Kevin Robinson, Liam Fedus, Denny Zhou, Daphne Ippolito, David Luan, Hyeontaek Lim, Barret Zoph, Alexander Spiridonov, Ryan Sepassi, David Dohan, Shivani Agrawal, Mark Omernick, Andrew M. Dai, Thanumalayan Sankaranarayanan Pillai, Marie Pellat, Aitor Lewkowycz, Erica Moreira, Rewon Child, Oleksandr Polozov, Katherine Lee, Zongwei Zhou, Xuezhi Wang, Brennan Saeta, Mark Diaz, Orhan Firat, Michele Catasta, Jason Wei, Kathy Meier-Hellstern, Douglas Eck, Jeff Dean, Slav Petrov, and Noah Fiedel. Palm: Scaling language modeling with pathways, 2022.
- [9] Danny Driess, Fei Xia, Mehdi SM Sajjadi, Corey Lynch, Aakanksha Chowdhery, Brian Ichter, Ayzaan Wahid, Jonathan Tompson, Quan Vuong, Tianhe Yu, et al. Palme: An embodied multimodal language model. *arXiv preprint arXiv:2303.03378*, 2023.
- [10] Yuqing Du, Olivia Watkins, Zihan Wang, Cédric Colas, Trevor Darrell, Pieter Abbeel, Abhishek Gupta, and Jacob Andreas. Guiding pretraining in reinforcement learning with large language models, 2023.
- [11] Frederik Ebert, Yanlai Yang, Karl Schmeckpeper, Bernadette Bucher, Georgios Georgakis, Kostas Daniilidis, Chelsea Finn, and Sergey Levine. Bridge data: Boosting generalization of robotic skills with cross-domain datasets, 2021.
- [12] Rishi Bommasani et al. On the opportunities and risks of foundation models, 2022.
- [13] Justin Fu, Katie Luo, and Sergey Levine. Learning robust rewards with adversarial inverse reinforcement learning. *arXiv preprint arXiv:1710.11248*, 2017.
- [14] Justin Fu, Avi Singh, Dibya Ghosh, Larry Yang, and Sergey Levine. Variational inverse control with events: A general framework for data-driven reward definition. *Advances in neural information processing systems*, 31, 2018.
- [15] Gemini Team Google. Gemini: A family of highly capable multimodal models, 2024.
- [16] Abhishek Gupta, Justin Yu, Tony Z. Zhao, Vikash Kumar, Aaron Rovinsky, Kelvin Xu, Thomas Devlin, and Sergey Levine. Reset-free reinforcement learning via multi-task learning: Learning dexterous manipulation behaviors without human intervention, 2021.
- [17] Jonathan Ho and Stefano Ermon. Generative adversarial imitation learning. *Advances in neural information processing systems*, 29, 2016.
- [18] Wenlong Huang, Pieter Abbeel, Deepak Pathak, and Igor Mordatch. Language models as zero-shot planners: Extracting actionable knowledge for embodied agents, 2022.
- [19] Wenlong Huang, Fei Xia, Ted Xiao, Harris Chan, Jacky Liang, Pete Florence, Andy Zeng, Jonathan Tompson, Igor Mordatch, Yevgen Chebotar, Pierre Sermanet, Noah Brown, Tomas Jackson, Linda Luu, Sergey Levine, Karol Hausman, and Brian Ichter. Inner monologue: Embodied reasoning through planning with language models, 2022.
- [20] Yunfan Jiang, Agrim Gupta, Zichen Zhang, Guanzhi

- Wang, Yongqiang Dou, Yanjun Chen, Li Fei-Fei, Anima Anandkumar, Yuke Zhu, and Linxi Fan. Vima: General robot manipulation with multimodal prompts. In *NeurIPS 2022 Foundation Models for Decision Making Workshop*, 2022.
- [21] Nikita Karaev, Ignacio Rocco, Benjamin Graham, Natalia Neverova, Andrea Vedaldi, and Christian Rupprecht. Cotracker: It is better to track together, 2023.
- [22] Ilya Kostrikov, Ashvin Nair, and Sergey Levine. Offline reinforcement learning with implicit q-learning. *arXiv preprint arXiv:2110.06169*, 2021.
- [23] Aviral Kumar, Aurick Zhou, George Tucker, and Sergey Levine. Conservative q-learning for offline reinforcement learning. *Advances in Neural Information Processing Systems*, 33:1179–1191, 2020.
- [24] Aviral Kumar, Anikait Singh, Frederik Ebert, Mitsuhiko Nakamoto, Yanlai Yang, Chelsea Finn, and Sergey Levine. Pre-training for robots: Offline rl enables learning new tasks from a handful of trials. *arXiv preprint arXiv:2210.05178*, 2022.
- [25] Junnan Li, Dongxu Li, Caiming Xiong, and Steven Hoi. Blip: Bootstrapping language-image pre-training for unified vision-language understanding and generation, 2022.
- [26] Raymond Li, Loubna Ben Allal, Yangtian Zi, Niklas Muennighoff, Denis Kocetkov, Chenghao Mou, Marc Marone, Christopher Akiki, Jia Li, Jenny Chim, Qian Liu, Evgenii Zheltonozhskii, Terry Yue Zhuo, Thomas Wang, Olivier Dehaene, Mishig Davaadorj, Joel Lamy-Poirier, João Monteiro, Oleh Shliazhko, Nicolas Gontier, Nicholas Meade, Armel Zebaze, Ming-Ho Yee, Logesh Kumar Umapathi, Jian Zhu, Benjamin Lipkin, Muhtasham Oblokulov, Zhiruo Wang, Rudra Murthy, Jason Stillerman, Siva Sankalp Patel, Dmitry Abulkhanov, Marco Zocca, Manan Dey, Zhihan Zhang, Nour Fahmy, Urvashi Bhattacharyya, Wenhao Yu, Swayam Singh, Sasha Luccioni, Paulo Villegas, Maxim Kunakov, Fedor Zhdanov, Manuel Romero, Tony Lee, Nadav Timor, Jennifer Ding, Claire Schlesinger, Hailey Schoelkopf, Jan Ebert, Tri Dao, Mayank Mishra, Alex Gu, Jennifer Robinson, Carolyn Jane Anderson, Brendan Dolan-Gavitt, Danish Contractor, Siva Reddy, Daniel Fried, Dzmitry Bahdanau, Yacine Jernite, Carlos Muñoz Ferrandis, Sean Hughes, Thomas Wolf, Arjun Guha, Leandro von Werra, and Harm de Vries. Starcoder: may the source be with you!, 2023.
- [27] Jacky Liang, Wenlong Huang, Fei Xia, Peng Xu, Karol Hausman, Brian Ichter, Pete Florence, and Andy Zeng. Code as policies: Language model programs for embodied control, 2023.
- [28] Fangchen Liu, Kuan Fang, Pieter Abbeel, and Sergey Levine. Moka: Open-vocabulary robotic manipulation through mark-based visual prompting, 2024.
- [29] Shilong Liu, Zhaoyang Zeng, Tianhe Ren, Feng Li, Hao Zhang, Jie Yang, Chunyuan Li, Jianwei Yang, Hang Su, Jun Zhu, and Lei Zhang. Grounding dino: Marrying dino with grounded pre-training for open-set object detection, 2023.
- [30] Yecheng Jason Ma, William Liang, Guanzhi Wang, De-An Huang, Osbert Bastani, Dinesh Jayaraman, Yuke Zhu, Linxi Fan, and Anima Anandkumar. Eureka: Human-level reward design via coding large language models. *arXiv preprint arXiv: Arxiv-2310.12931*, 2023.
- [31] Parsa Mahmoudieh, Deepak Pathak, and Trevor Darrell. Zero-shot reward specification via grounded natural language. In Kamalika Chaudhuri, Stefanie Jegelka, Le Song, Csaba Szepesvari, Gang Niu, and Sivan Sabato, editors, *Proceedings of the 39th International Conference on Machine Learning*, volume 162 of *Proceedings of Machine Learning Research*, pages 14743–14752. PMLR, 17–23 Jul 2022. URL <https://proceedings.mlr.press/v162/mahmoudieh22a.html>.
- [32] Max Sobol Mark, Ali Ghadirzadeh, Xi Chen, and Chelsea Finn. Fine-tuning offline policies with optimistic action selection. In *Deep Reinforcement Learning Workshop NeurIPS 2022*, 2022.
- [33] Matthias Minderer, Alexey Gritsenko, Austin Stone, Maxim Neumann, Dirk Weissenborn, Alexey Dosovitskiy, Aravindh Mahendran, Anurag Arnab, Mostafa Dehghani, Zhuoran Shen, Xiao Wang, Xiaohua Zhai, Thomas Kipf, and Neil Houlsby. Simple open-vocabulary object detection with vision transformers, 2022.
- [34] Suvir Mirchandani, Fei Xia, Pete Florence, Brian Ichter, Danny Driess, Montserrat Gonzalez Arenas, Kanishka Rao, Dorsa Sadigh, and Andy Zeng. Large language models as general pattern machines. *arXiv preprint arXiv:2307.04721*, 2023.
- [35] Mitsuhiko Nakamoto, Yuexiang Zhai, Anikait Singh, Max Sobol Mark, Yi Ma, Chelsea Finn, Aviral Kumar, and Sergey Levine. Cal-ql: Calibrated offline rl pre-training for efficient online fine-tuning. In *Neural Information Processing Systems (NeurIPS)*, 2023.
- [36] Soroush Nasiriany, Fei Xia, Wenhao Yu, Ted Xiao, Jacky Liang, Ishita Dasgupta, Annie Xie, Danny Driess, Ayzaan Wahid, Zhuo Xu, et al. Pivot: Iterative visual prompting elicits actionable knowledge for vlms. *arXiv preprint arXiv:2402.07872*, 2024.
- [37] OpenAI. Gpt-4 technical report, 2024.
- [38] Alec Radford, Jong Wook Kim, Chris Hallacy, Aditya Ramesh, Gabriel Goh, Sandhini Agarwal, Girish Sastry, Amanda Askell, Pamela Mishkin, Jack Clark, Gretchen Krueger, and Ilya Sutskever. Learning transferable visual models from natural language supervision, 2021.
- [39] Tianhe Ren, Shilong Liu, Ailing Zeng, Jing Lin, Kunchang Li, He Cao, Jiayu Chen, Xinyu Huang, Yukang Chen, Feng Yan, Zhaoyang Zeng, Hao Zhang, Feng Li, Jie Yang, Hongyang Li, Qing Jiang, and Lei Zhang. Grounded sam: Assembling open-world models for diverse visual tasks, 2024.
- [40] Archit Sharma, Kelvin Xu, Nikhil Sardana, Abhishek Gupta, Karol Hausman, Sergey Levine, and Chelsea Finn. Autonomous reinforcement learning: Formalism

- and benchmarking, 2022.
- [41] Avi Singh, Larry Yang, Kristian Hartikainen, Chelsea Finn, and Sergey Levine. End-to-end robotic reinforcement learning without reward engineering. *arXiv preprint arXiv:1904.07854*, 2019.
- [42] Charles Sun, Jędrzej Orbik, Coline Manon Devin, Brian H. Yang, Abhishek Gupta, Glen Berseth, and Sergey Levine. Fully autonomous real-world reinforcement learning with applications to mobile manipulation. In Aleksandra Faust, David Hsu, and Gerhard Neumann, editors, *Proceedings of the 5th Conference on Robot Learning*, volume 164 of *Proceedings of Machine Learning Research*, pages 308–319. PMLR, 08–11 Nov 2022. URL <https://proceedings.mlr.press/v164/sun22a.html>.
- [43] Marcel Torne, Max Balsells, Zihan Wang, Samedh Desai, Tao Chen, Pulkit Agrawal, and Abhishek Gupta. Bread-crumbs to the goal: Goal-conditioned exploration from human-in-the-loop feedback, 2023.
- [44] Andrés Villa, Juan León Alcázar, Motasem Alfarra, Kmail Alhamoud, Julio Hurtado, Fabian Caba Heilbron, Alvaro Soto, and Bernard Ghanem. Pivot: Prompting for video continual learning, 2023.
- [45] Homer Walke, Kevin Black, Abraham Lee, Moo Jin Kim, Max Du, Chongyi Zheng, Tony Zhao, Philippe Hansen-Estruch, Quan Vuong, Andre He, Vivek Myers, Kuan Fang, Chelsea Finn, and Sergey Levine. Bridgedata v2: A dataset for robot learning at scale. In *Conference on Robot Learning (CoRL)*, 2023.
- [46] Yen-Jen Wang, Bike Zhang, Jianyu Chen, and Koushil Sreenath. Prompt a robot to walk with large language models. *arXiv preprint arXiv:2309.09969*, 2023.
- [47] Annie Xie, Avi Singh, Sergey Levine, and Chelsea Finn. Few-shot goal inference for visuomotor learning and planning. In *Conference on Robot Learning*, pages 40–52. PMLR, 2018.
- [48] Haoyu Xiong, Russell Mendonca, Kenneth Shaw, and Deepak Pathak. Adaptive mobile manipulation for articulated objects in the open world. *arXiv preprint arXiv:2401.14403*, 2024.
- [49] Jiarui Xu, Sifei Liu, Arash Vahdat, Wonmin Byeon, Xiaolong Wang, and Shalini De Mello. Open-vocabulary panoptic segmentation with text-to-image diffusion models, 2023.
- [50] Jianwei Yang, Hao Zhang, Feng Li, Xueyan Zou, Chunyuan Li, and Jianfeng Gao. Set-of-mark prompting unleashes extraordinary visual grounding in gpt-4v. *arXiv preprint arXiv:2310.11441*, 2023.
- [51] Jingyun Yang, Max Sobol Mark, Brandon Vu, Archit Sharma, Jeannette Bohg, and Chelsea Finn. Robot fine-tuning made easy: Pre-training rewards and policies for autonomous real-world reinforcement learning. *Conference on Robot Learning (CoRL)*, 2023.
- [52] Zhengyuan Yang, Linjie Li, Kevin Lin, Jianfeng Wang, Chung-Ching Lin, Zicheng Liu, and Lijuan Wang. The dawn of lmms: Preliminary explorations with gpt-4v(ision), 2023.
- [53] Wenhao Yu, Nimrod Gileadi, Chuyuan Fu, Sean Kirmani, Kuang-Huei Lee, Montse Gonzalez Arenas, Hao-Tien Lewis Chiang, Tom Erez, Leonard Hasenclever, Jan Humplik, Brian Ichter, Ted Xiao, Peng Xu, Andy Zeng, Tingnan Zhang, Nicolas Heess, Dorsa Sadigh, Jie Tan, Yuval Tassa, and Fei Xia. Language to rewards for robotic skill synthesis, 2023.
- [54] Deyao Zhu, Jun Chen, Xiaoqian Shen, Xiang Li, and Mohamed Elhoseiny. Minigpt-4: Enhancing vision-language understanding with advanced large language models, 2023.

APPENDIX

A. Experiments to Verify Reproduction of RoboFuME

Demonstrating success rates on the cloth tasks comparable to the RoboFuME results was a positive indicator for successful reproduction of the online RL pipeline. However, based on the results in Table IV, failure to achieve similar results on the Spatula Pick-Place pretrained offline RL policy on Bridge data and high-quality in-domain demonstrations, regardless of the Bridge data subset used, suggests that generalizing the online RL pipeline to new tasks is challenging.

Our ablation experiments in Table III demonstrated that without in-domain data, all policy variants struggled to get any meaningful learning signal on every task. Furthermore, a preliminary experiment finetuning the offline RL policy pretrained only on Bridge data demonstrated challenges learning with sparse rewards achieves barely any increase in success rates (column 6 of Table I). Therefore, we hypothesized that with dense shaping rewards, policies pretrained on both dense and sparse rewards would struggle to learn during online finetuning, and we were unlikely to achieve meaningful success rates on Spatula Pick-Place without in-domain demonstrations. While RoboFuME has demonstrated interesting results in reducing human effort in reward engineering and resets, there is a notable cost incurred with collecting in-domain demonstrations for each new task. In-domain demonstrations are crucial for policies pretrained offline to succeed in task transfer to new environments, as seen in the following experiments. In-domain demonstrations are also crucial for finetuning MiniGPT-4 to yield accurate sparse task completion rewards.

To avoid confounding generalization issues and to verify successful reproduction of the pipeline, we picked two tasks in the RoboFuME task suite that performed well, Cloth Folding (Figure 4) and Cube Covering (Figure 5). On both tasks, language-conditioned policies pretrained with behavior cloning (BC) and offline RL had decent success rates, which improved with online finetuning. To test the necessity of in-domain demonstrations for the success of the pipeline, for each task we pretrained four policies: language-conditioned BC on Bridge data and in-domain demonstrations, offline on Bridge data and in-domain demonstrations, language-conditioned BC on Bridge data only, and offline RL on Bridge data. We used the same Bridge data subsets as RoboFuME for each task, with newly collected in-domain demonstrations using our setup. We evaluated the four policies on the forward and backward tasks for each task category, and the results are shown in Table III.

Similar to Yang et al. [51], we report the success rates for the forward tasks only. We successfully reproduced the results of RoboFuME for the BC and RL policies trained on both Bridge and in-domain data (see the first two columns of Table I in [51]). However, removing in-domain demonstration data from the pretraining dataset was catastrophic for policy learning, resulting in zero successes for both task categories. This confirms the heavy reliance of the RoboFuME pipeline on in-domain demonstrations.

Task	BC bridge only	RL bridge only	BC bridge + indomain	RL bridge + indomain
Cloth Folding	0%	0%	65%	70%
Cube Covering	0%	0%	35%	55%

TABLE III: Success rates for Cloth Folding and Cube Covering tasks, on 20 trials of each task.

In-domain demonstrations are crucial for both aspects of the RoboFuME pipeline: pretraining policies with language-conditioned BC or offline RL as well as finetuning the task classifier that yields sparse rewards. It is not scalable to collect in-domain demonstrations for every new task we care about. Furthermore, the pipeline required in-domain demonstrations to meet several constraints, such as minimizing multimodality in the demonstrations, and if at evaluation or during finetuning there are any differences in the environment (e.g., lighting changes, changes in object position, changes in background), the system is very likely to fail. Overall, these experiments demonstrate reliance on in-domain demonstrations for transfer to new environments makes the system highly brittle, evidenced by the ablation experiments conducted that pretrained policies only on Bridge data without the in-domain demos resulting in zero success on all tasks. Therefore, while RoboFuME reduces human effort in reward specification and resets, collecting demonstrations is still a bottleneck for this method, both in human effort and in the fragility of the system.

The experiments also demonstrate the challenges of relying on high-quality in-domain demonstrations with low multimodality to successfully pretrain policies for online RL. Such pipelines are made much more brittle and less robust to generalizing to new tasks, objects, and environments. It is possible that a combination of selecting a highly task-relevant subset of the Bridge dataset facilitating good transfer to the current task and improved hyperparameter tuning for CalQL could have enabled the system to learn via online finetuning with dense rewards without needing any in-domain demonstrations at all, but this would require much more extensive further exploration in this direction in both pretraining data selection and hyperparameter search for online RL. A broader goal of subsequent research in this area would be to develop online RL methods that are much less reliant on or completely eliminate the need for in-domain demonstrations, and able to more effectively extract useful priors from offline datasets like Bridge datasets during pretraining, in addition to improving finetuning methods.

B. Selecting Pretraining Data for Spatula Pick-Place

Pretraining on the entire Bridge dataset would be computationally and practically infeasible. As such, choosing subsets of prior datasets to train on is crucial for downstream performance. We test this with a novel Spatula Pick-Place task that is not part of the list of RoboFuME tasks. We define the forward task to be `put spatula on plate` and the backward task to be `move spatula to the left of the plate`, formatting language descriptions similar to those in the Bridge dataset, demonstrated in the image

sequences in Figure 6. We consider three different subsets of Bridge data. `tabletop granular` comprises 796 trajectories performing tasks on a tabletop similar to the one used in our experiments. `tabletop granular + toy kitchen` comprises 823 trajectories, with `toy kitchen` trajectories specifically focusing on pick and place tasks with a variety of objects. `tabletop granular + toy kitchen + dark wood` comprises 1764 trajectories, with `dark wood` trajectories including some spatula pick and place tasks similar to ours, among many other tasks. We pretrain three separate policies using offline RL on each of the Bridge data combinations, as well as 120 in-domain demonstrations (50 forward task rollouts, 50 backward task rollouts, and 20 failures), as done in RoboFuME. The results of evaluating the three policies on the forward and backward tasks are shown in Table IV.

Task	tabletop	tabletop + toy kitchen	tabletop + toy kitchen + dark wood
Forward	20%	10%	5%
Backward	25%	10%	10%

TABLE IV: Success rates on forward and backward task for Spatula Pick-Place using different subsets of Bridge data, on 20 trials of each task.

From these results, we observe that increasing the size and diversity of the pretraining dataset does not necessarily lead to better results on the task, in fact it is the opposite. Qualitative analysis of the pick and place behavior shows a similar declining trend with more Bridge data. Even when adding the `dark wood` dataset which has the same task in the dataset, the performance is the worst among the three subset combinations. This demonstrates the importance of pretraining data selection for the performance of the eventual policy.

We noted that the success rates for the novel Spatula Pick-Place task was much lower than the reported success rates in [51], suggesting issues with generalization capabilities of the pipeline. We also observed that RoboFuME codebase not only pretrains on Bridge data, but also in-domain demonstration data that is upsampled by 8x to be proportional to the size of Bridge data. This could explain the observed results that increasing the size of pretraining Bridge datasets causes worse performance, because it dilutes the upsampled in-domain data. This demonstrates that the RoboFuME pipeline is heavily dependent on in-domain demonstrations to succeed. We test the effect of these demonstrations in Appendix A.

From our experiments selecting different pretraining datasets for the novel Spatula Pick-Place, the selection of prior offline datasets is incredibly important for downstream success of the pretrained policy. It might be unique to the RoboFuME pipeline that smaller prior datasets are better to avoid diluting the in-domain demonstration data, and the optimal selection of prior data could have greatly improved both the pretrained policy and finetuned policy’s performance. However, it is still surprising that including demonstrations of the exact task being evaluated on (though in a different environment) does

not help with task completion. More research into extracting relevant data from prior datasets can alleviate this issue.

C. Simulation Experiments for Dense Reward Formulation

We conduct preliminary experiments in simulation to investigate the effects of finetuning with a dense reward. In simulation, the dense reward is naively the negative L2 distance between the robot and the target location. We further investigate whether using a dense reward formulation can reduce the reliance of the policy on in-domain demonstrations during policy pretraining. The results of the simulation experiments for policies using the standard number of in-domain demonstrations, including the reproduction of the RoboFuME pipeline, can be seen in Figure 8.



(a) Standard quantity of in-domain demonstrations, sparse reward only (RoboFuME).



(b) Standard quantity of in-domain demonstrations, dense and sparse rewards.

Fig. 8: Evaluation metrics of policies trained on the standard number of in-domain demonstrations, using sparse only or dense and sparse rewards. From left to right: average episode length, success rate, average episode reward.

We see in Figure 8 that adding the dense reward generally performs comparably, verifying our dense reward formulation is sensible. To determine whether one of these reward formulations, sparse only (as done in RoboFuME) vs. dense and sparse, is more adversely affected by reducing the number of in-domain demonstrations during pretraining, we conduct two simulation experiments for policies using fewer in-domain demonstrations, specifically half the pretraining data compared to the standard quantity, for which the results are shown in Figure 9. We see that these also perform comparably with each other and with the previous experiment using the standard number of in-domain demonstrations. The dense and sparse reward formulation reaches higher success rates slightly faster despite fewer in-domain demonstrations. Due to the dense rewards in simulation only being approximated with a single waypoint at the target location, we believe a denser waypoint trajectory should help with learning on the real robot, with the simulation experiments verifying that adding dense rewards at least does not hurt or inhibit learning, and potential for learning on the real robot setup.

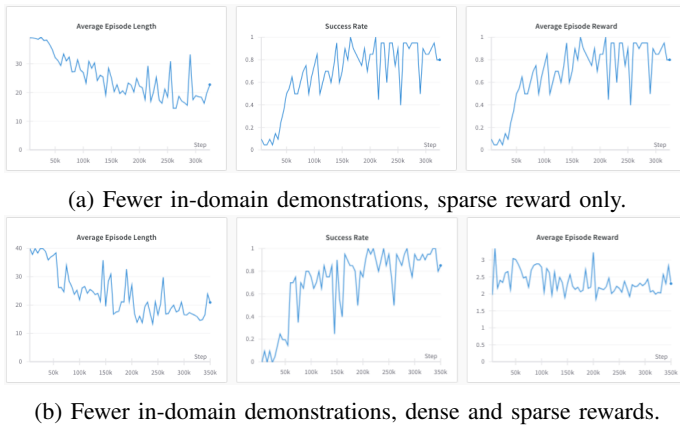


Fig. 9: Evaluation metrics of policies trained on fewer in-domain demonstrations, using sparse only or dense and sparse rewards. From left to right: average episode length, success rate, average episode reward.

D. Qualitative Observations of VLM Performance

The success of the online RL system is highly dependent on the accuracy of VLM keypoint and waypoint predictions for task completion, as inaccuracies in these predictions lead to suboptimal reward shaping and hinder the learning process, or even cause the learning of wrong behaviors. Below we include a short commentary on empirical observations of VLM performance. The VLMs investigated were GPT-4V (also used by Liu et al. [28]), Gemini Pro, and GPT-4o. We tested the outputs of these models on the three tasks described above: Cloth Folding, Cube Covering, Spatula Pick-Place, as well as some additional tasks from RoboFuME to verify the robustness of the system such as Candy Sweeping, Drawer Opening, and pick and place tasks using other objects in a toy kitchen setup. We provide the task descriptions and metaprompts in E.

First, we observe that the natural language description of the task is important for facilitating the correct waypoint generation. For example, for Spatula Pick-Place, the backward task phrased as "Place the spatula on the left of the plate" sometimes led to waypoints generated in a way that moves the spatula to the left side of the yellow plate (but still on the plate), rather than on the table on the left side of the plate. We had to tune the natural language descriptions as such. Tuning typically occurred on the level of the specific task description, and the meta-prompt required some modifications from Liu et al. [28] to generate the intended outputs, but once tuned remained consistent for all experiments. Once tuned, for the three tasks reported above, manual inspection of the VLM outputs indicate that the outputs are generally reliable and consistent across trials for the top-down perspective, the perspective used in our real robot experiments.

Another observation is for the approach of providing dual-angle inputs to VLMs, where the side-view of the environment was also provided to the system. Gemini tends to perform slightly better than the GPT models in 3D spatial reasoning and generating depth information that facilitates successful

completion of the task. The GPT models, GPT-4V in particular, sometimes struggles to generate sensible depth movements from the side angle to facilitate e.g. pick and place of the spatula. This observation would be important for extensions of this work investigating 3D waypoint generation, as depth information is critical for pick and plac, tasks performed on uneven surfaces, as well as tasks with very specific grasp points like drawer opening.

Our experiments and empirical observations verify the hypotheses in Liu et al. [28] that state-of-the-art VLMs are capable of spatial reasoning at a sufficient accuracy to facilitate tabletop manipulation tasks of various complexities, where a top-down and side view of the environment gives sufficient information to perform the tasks. We anticipate that the spatial reasoning of VLMs will only continue to improve, and more studies can be conducted in mobile or open-world manipulation, to see whether the spatial reasoning capabilities of VLMs extend to even more complex and dynamic environments beyond tabletop manipulation.

E. GPT-4V Prompts

1) *Task Descriptions:* Below are the task descriptions used for testing VLM waypoint generation. Note that for our system, task descriptions must be specific as the forward and backward tasks must be near inverses of each other and move objects to specific positions for reset-free RL to work smoothly. For object manipulation outside the reset-free setting, this level of specificity may not be required, and more "natural" language instructions can be provided to VLMs.

Spatula Pick-Place:

- 1) Forward: Place the spatula on the plate.
- 2) Backward: Move the spatula to the table on the left of the plate.

Cloth Folding:

- 1) Forward: Fold the cloth from left to right.
- 2) Backward: Unfold the cloth from right to left.

Cube Covering:

- 1) Forward: Cover the box with the cloth from left to right.
- 2) Backward: Uncover the box beneath the cloth from right to left.

Candy Sweeping:

- 1) Forward: Sweep the candies from the left side of the tray to the right side.
- 2) Backward: Sweep the candies from the right side of the tray to the left side.

Drawer Opening/Closing:

- 1) Forward: Open the drawer.
- 2) Backward: Close the drawer.

Toy Kitchen Pick-Place:

- 1) Forward: Place the pot in the center of the sink.
- 2) Backward: Place the pot on the dish rack.

2) *Metaprompt for Sparse Reward Generation*: Given the task instruction and the image, has the task been completed in this image from the camera’s perspective? Answer ‘yes’ or ‘no’, do not explain your reasoning.

3) *Metaprompt for Waypoint Generation*: The metaprompt below was largely inspired by the metaprompt using by MOKA [28], modified to generate the dense waypoint trajectory required for our project. We have tested this metaprompt with a variety of models, including Gemini Pro and GPT-4o, and this metaprompt is suitable for use with other models with comparable performance to GPT-4V, as of June 2024.

Describe the robot gripper’s motion to solve the task by selecting pre-defined keypoints and waypoints. The input request contains:

- The task information as dictionaries. The dictionary contains these fields:

- * ‘instruction’: The task in natural language forms.

- * ‘object_grasped’: The object that the robot gripper will hold in hand while executing the task.

- * ‘object_unattached’: The object that the robot gripper will interact with either directly or indirectly via ‘object_grasped’.

- An image of the current table-top environment captured from a top-down camera, annotated with a set of visual marks:

- * candidate keypoints on ‘object_grasped’: Purple dots marked as ‘P[i]’ on the image, where [i] is an integer.

- * candidate keypoints on ‘object_unattached’: Green dots marked as ‘Q[i]’ on the image, where [i] is an integer.

- * grid for waypoints: Grid lines that uniformly divide the images into tiles. The grid equally divides the image into columns marked as ‘a’, ‘b’, ‘c’, ‘d’, ‘e’, ‘f’, ‘g’ from left to right and rows marked as 1, 2, 3, 4, 5 from bottom to top.

- * start point of gripper: Red dot marking the starting position of the gripper.

- * start point of ‘object_grasped’: Blue dot marking the starting position of ‘object_grasped’.

- An image of the current table-top environment captured from a side view camera, annotated with a set of visual marks:

- * horizontal gridlines: Grid lines that uniformly divide the image from bottom to top, where each line represents height from the tabletop. The grid equally divides the image into segments marked as ‘z1’, ‘z2’, ‘z3’, ‘z4’, ‘z5’, ‘z6’, ‘z7’, ‘z8’ from bottom to top.

- * start point of gripper: Red dot marking the starting position of the gripper.

- * start point of ‘object_grasped’: Blue dot marking the starting position of ‘object_grasped’.

The motion consists of a grasping phase and a manipulation phase, specified by ‘grasp_keypoint’, ‘function_keypoint’, ‘target_keypoint’, ‘pre_contact_waypoint’, ‘post_contact_waypoint’.

Please note: In the grasping phase, the robot gripper sequentially moves to the ‘pre_contact_waypoint’ and grasps ‘object_grasped’ at the ‘grasp_keypoint’. In the manipulation phase, the robot gripper moves to ‘post_contact_waypoint’

first, then moves the ‘function_keypoint (or ‘object_grasped’ if ‘function_keypoint’ is ‘’) to ‘target_keypoint’, performing a motion trajectory that completes the task instruction by first completing the grasping phase then the manipulation phase.

More specifically, the definitions of these points are:

- ‘grasp_keypoint’: The point on ‘object_grasped’ indicates the part where the robot gripper should hold.

- ‘function_keypoint’: The point on ‘object_grasped’ indicates the part that will make contact with ‘object_unattached.’

- ‘target_keypoint’: If the task is pick-and-place, this is the location where ‘object_grasped’ will be moved to. Otherwise, this is the point on ‘object_unattached’ indicating the part that will be contacted at the end of the motion by ‘function_keypoint’, or the robot gripper (if ‘function_keypoint’ is ‘’).

- ‘pre_contact_waypoint’: The waypoint in the free space that the robot gripper moves to before making contact with the ‘grasp_keypoint’.

- ‘post_contact_waypoint’: The waypoint in the free space that the robot gripper moves to after making contact with the ‘grasp_keypoint’, before moving ‘function_keypoint’ (or ‘object_grasped’ if ‘function_keypoint’ is ‘’) to ‘target_keypoint’. The response should be a dictionary in JSON form, which contains:

- ‘grasp_keypoint’: Selected from candidate keypoints marked as ‘P[i]’ on the image. This will be ‘’ if and only if ‘object_grasped’ is ‘’.

- ‘function_keypoint’: Selected from candidate keypoints marked as ‘P[i]’ on the image. This will be ‘’ if and only if ‘object_grasped’ or ‘object_unattached’ is ‘’ or the task is pick-and-place.

- ‘target_keypoint’: Selected from keypoint candidates marked as ‘Q[i]’ on the image. This will be ‘’ if and only if ‘object_unattached’ is ‘’.

- ‘start_block’: A tuple ([pos], [height]): [pos] is the tile where the robot gripper (marked by a red dot) is located, which is selected from candidate tiles ‘[x][i]’ marked on the first top-down image, where [x] is the column index as a lower letter and [i] is the row index as an integer. [height] is the line representing the height of the robot gripper, which is selected from candidate lines ‘z[i]’ marked on the second side view image, where [i] is the line index as an integer.

- ‘grasp_block’: A tuple ([pos], [height]): [pos] is the tile where the robot gripper grasps the object at ‘grasp_keypoint’, which is selected from candidate tiles ‘[x][i]’ marked on the first top-down image, where [x] is the column index as a lower letter and [i] is the row index as an integer. [height] is the line representing the height of the grasped object, which is selected from candidate lines ‘z[i]’ marked on the second side view image, where [i] is the line index as an integer.

- ‘target_block’: A tuple ([pos], [height]): [pos] is the tile where ‘target_keypoint’ is currently located in, which is selected from candidate tiles ‘[x][i]’ marked on the first top-down image, where [x] is the column index as a lower letter and [i] is the row index as an integer. [height] is the line representing the height of the target location, which is selected

from candidate lines 'z[i]' marked on the second side view image, where [i] is the line index as an integer.

- 'block_sequence': A list of tuples of the form ([pos], [height]), where [pos] is selected from candidate tiles '[x][i]' marked on the first top-down image, where [x] is the column index as a lower letter and [i] is the row index as an integer, and [height] is selected from candidate lines 'z[i]' marked on the second side view image, where [i] is the line index as an integer. The list of tuples represents the locations that the robot gripper should move to sequentially to complete the task. Remember that the robot gripper first completes the grasping phase by moving to 'pre_contact_waypoint' and grasping 'object_grasped' at the 'grasp_keypoint'. Next, in the manipulation phase, the robot gripper moves to 'post_contact_waypoint' first, then moves the 'function_keypoint (or 'object_grasped' if 'function_keypoint' is '') to 'target_keypoint', performing a motion trajectory that completes the task instruction by first completing the grasping phase then the manipulation phase. Think about this step by step: the list should begin with 'start_block', navigate to 'grasp_block', and end with 'target_block'. The elements of the list should be tuples of the form ([pos], [height]), where [pos] is selected from candidate tiles '[x][i]' marked on the first top-down image, where [x] is the column index as a lower letter and [i] is the row index as an integer, and [height] is selected from from candidate lines 'z[i]' marked on the second side view image, where [i] is the line index as an integer. Furthermore, as 'block_sequence' is sequentially generated starting with 'start_block', from the last element ([pos1], [height1]) in the sequence so far, the next block ([pos2], [height2]) is generated as follows: first generate [pos2] by choosing one of the eight tiles surrounding the current tile [pos1] (up, up-left, up-right, left, right, down, down-left, down-right), then generate [height2] by choosing the line above, below, or the same as the current line [height1]. The next tile should be chosen in a way that the resultant motion in 3D can be followed by the robot gripper to first complete the grasping phase, then after a successful grasp, complete the manipulation phase, thereby completing the task instruction with collision avoidance and all proper contacts made. This sequence generation process continues until the last tile in the sequence so far 'target_block', which is when the robot gripper's motion is completed. Double check that for each consecutive block of format ([pos], [height]), [pos] is reachable from the previous [pos] by moving either up, up-left, up-right, left, right, down, down-left, down-right, and [height] is reachable from the previous [height] by moving up, down, or staying the same.

- 'pre_contact_height': The height of 'pre_contact_waypoint' as one of the two options 'same' (same as the height of making contact with 'target_keypoint') or 'above' (higher than the height of making contact with 'target_keypoint').

- 'post_contact_height': The height of 'post_contact_waypoint' as one of the two options 'same' (same as the height of making contact with 'target_keypoint')

or 'above' (higher than the height of making contact with 'target_keypoint').

- 'target_angle': Describe how the object should be oriented during this motion in terms of the axis pointing from the grasping point to the function point. Think about this step by step. First analyze whether this axis should be parallel with or perpendicular to the motion direction and the table surface respectively to better perform the task, then choose the axis orientation from one of these strings based on the motion direction: 'forward' (toward the top side of the image), 'backward' (toward the bottom side of the image), 'upward' (perpendicular to and away from the table surface), 'downward' (perpendicular to and towards the table surface), 'left' (towards the left side of the image), 'right' (towards the right side of the image). e.g., if the axis is parallel to the table surface and perpendicular to the motion direction, and the motion direction is backward, then the axis direction should be either 'left' or 'right'; if the axis is perpendicular to the table surface and parallel to the motion direction, and the motion direction is upward, then the axis direction should be either 'upward' or 'downward'.

We will first provide one in-context example, which contains the input (the corresponding task instruction and pair of input images (top-down and side view)), and the correct response. Then we will provide a new task instruction and pair of input images (top-down and side view) and ask for the corresponding response based on the in-context example.

Think about this step by step: First, choose 'grasp_keypoint', 'function_keypoint', and 'target_keypoint' on the correct parts of the objects. Next, determine which block the robot gripper is in ('start_block'), which block the 'grasp_keypoint' is located in ('grasp_block'), and which block the 'target_keypoint' is located in ('target_block'). Then generate 'block_sequence' (starting with 'start_block', moving through some sequence of blocks to 'grasp_block', then moving through another sequence of blocks and ending with 'target_block') and choose 'pre_contact_height', 'post_contact_height' accordingly such that the robot gripper's resultant motion of 'pre_contact_waypoint' → 'grasp_keypoint' → 'post_contact_waypoint' then moving 'function_keypoint' (or 'object_grasped' if 'function_keypoint' is '') to the 'target_waypoint' in 3D completes the grasping phase first then the manipulation phase and proper contacts will be made. Remember that in the first top-down image, the columns are marked as 'a', 'b', 'c', 'd', 'e', 'f', 'g' from left to right, and the rows are marked as 1, 2, 3, 4, 5 from bottom to top; in the second side view image, the lines are labeled 'z1', 'z2', 'z3', 'z4', 'z5', 'z6', 'z7', 'z8' from bottom to top. Explain the reasoning steps.